

Adaptive oscillatory neurons generate periodic bursting: analytic and numerical study of the attractor dynamics

Tanguy Fardet, Mathieu Ballandras, Samuel Bottani, Stéphane Métens, Pascal Monceau

▶ **To cite this version:**

Tanguy Fardet, Mathieu Ballandras, Samuel Bottani, Stéphane Métens, Pascal Monceau. Adaptive oscillatory neurons generate periodic bursting: analytic and numerical study of the attractor dynamics. 2016. hal-01401843v1

HAL Id: hal-01401843

https://hal.science/hal-01401843v1

Preprint submitted on 23 Nov 2016 (v1), last revised 13 Feb 2024 (v2)

HAL is a multi-disciplinary open access archive for the deposit and dissemination of scientific research documents, whether they are published or not. The documents may come from teaching and research institutions in France or abroad, or from public or private research centers.

L'archive ouverte pluridisciplinaire **HAL**, est destinée au dépôt et à la diffusion de documents scientifiques de niveau recherche, publiés ou non, émanant des établissements d'enseignement et de recherche français ou étrangers, des laboratoires publics ou privés.



Distributed under a Creative Commons Attribution 4.0 International License

Adaptive oscillatory neurons generate periodic bursting: analytic and numerical study of the attractor dynamics.

Tanguy Fardet,[1] Mathieu Ballandras,[1] Samuel Bottani,[1] Stéphane Métens,[1] and Pascal Monceau[1,2]

[1] *Laboratoire Matière et Systèmes Complexes, Université Paris 7 – Diderot, 5 rue Thomas-Mann 75205 Paris cedex 13, France*

[2] *Université d'Evry-Val d'Essonne, France*

Several experimental and numerical studies have observed that populations of oscillatory neurons can synchronize and converge to an dynamical attractor composed of periodic bursts which involve the whole network. We show here that a sufficient condition for this phenomenon to occur is the presence of an excitatory population of oscillatory neurons displaying spike-driven adaptation, which was observed for cultured pyramidal neurons from the cortex or the hippocampus. More than just synchronization – which takes place even for weak coupling – bursting occurs for stronger coupling as the adaptive neurons switch from their initial adaptive spiking to an intermittent burst-like behavior. Addition of inhibitory neurons or plastic synapses can then modulate this dynamics in many ways but is not necessary for its appearance. After discussing the origin of the bursting behavior, we provide a detailed analytic and numerical description of such dynamics, as well as the evolution of its properties depending on the neuronal and synaptic parameters. This allows us to explain the change in the neuronal dynamics and the phenomenon underlying the termination of a burst. We based our study on a mean-field model for adaptive exponential integrate-and-fire (aEIF or AdEx) neurons, thanks to which we discuss the related biological phenomena and the relevance of the explored region of parameter space.

Keywords: Bursting | Adaptation | Neuronal networks | Synchronicity | Oscillators

Significance statement

A sufficient condition for synchronous bursting in neuronal population is the existence of a population of excitatory neurons displaying spike-driven adaptation and oscillatory behavior. For strong enough coupling, the adaptive neurons not only synchronize but switch from their initial regular spiking to an emergent and intermittent burst-like behavior. Using a 2D dynamical system, we provide a detailed analytic and numerical description of such dynamics based on a simplified mean-field model. This leads to a minimal model, based on a hypothesis that can be tested experimentally, which not only reproduces the biological observations but also provides an explanation to the underlying phenomena involved in synchronous bursting. Indeed we propose possible mechanisms for both the initiation and termination of a collective burst as well as analytic results to predict the properties of the global activity and its evolution depending on neuronal and synaptic parameters.

INTRODUCTION

Characterizing the different forms of organized spatio-temporal behavior in neuronal populations and how they emergence is a fundamental endeavor towards understanding neuronal systems and the brain. Therefore, the study of synchronization in neuronal activity, or of other forms of correlated behavior between neurons, has been a long-standing active field for experimental and theoretical investigations.

Collective periodic bursting of a neuronal population is an intermittent behavior composed of long periods of rest where almost no spikes are emitted, which are punctuated by brief periods of intense activity, characterized by very high firing rates over the whole network. It is a well know phenomenon both in brain regions and neuronal cultures, and it has been investigated as a plausible candidate for rhythmogenesis [1], but also in various disorders such as epilepsy or Parkinson. As will be detailed in the following parts, the activity of the neurons during the active window – the *burst* – is composed of at least 2 closely-packed spikes.

This work was inspired by recent experiments [2] which, by controlling precisely the chemical environment of a culture revealed that the spontaneous bursting phenomenon could be extremely regular, with a well defined period, contrary to the usual recordings in less controlled media.

We therefore took this work as a starting point of our model, then aimed at reproducing and explaining several other experimental observations [3–5] exhibiting different bursting behaviors, with inter-burst intervals (IBIs) ranging from less than one second up to several minutes.

We will not try to describe the transition of the neuronal population from an asynchronous to a synchronized phase, but will directly consider the synchronized state, whose underlying mechanisms we try to uncover.

Let us insist on the fact that collective bursting should not be confused with the individual behavior observed for "bursting" or "chattering" neuron types at the cellular level. Though they share similar intervals of rapid firing followed by long quiet periods [3, 6, 7], hence the common name, collective bursting can stem from radically different mechanisms and occur on different timescales.

More specifically, in our description, population-wide bursts are a special form of synchronized behavior which emerges from the interactions of individual adaptive-spiking neurons on a network, which do not display individual bursting behavior, but only emit one spike at a time.

By adaptation, we refer at the capacity of a neuron to change – here, more precisely, to lower – its excitability in response to continuous or repeated excitation, such as a step-current in electrophysiological experiments, or the intense synaptic input received from its neighbors during a collective burst.

We show here that adaptive spiking is a sufficient condition for this bursting phenomenon to occur, and that intrinsically bursting or chattering neurons are not required. Indeed, we focus on the role of adaptation to explain why, as observed in the experiments, the presence of inhibitory neurons is not necessary to obtain regular collective bursting dynamics. Likewise, though short-term synaptic plasticity might play a role in shaping the dynamics [5, 8, 9], we also demonstrate that it is not required to reproduce characteristic timescales of this dynamics.

METHODS

We first describe the models used for the different units composing the system (neurons, synapses and network structure). Based on these, we build our theoretical model by developing a mean-field approach that remains almost completely tractable so that most of the properties of the collective dynamics can be obtained analytically. This model is based on successive approximations that remain in agreement with numeric simulations. We also used these numeric simulations to verify and extend the predictions of our analytic mean-field model.

Neuronal model

We chose the adaptive Exponential Integrate-and-Fire (aEIF) model [10] because of its compromise between simplicity and biological relevance. The dynamical evolution of a neuron is described by two variables, its membrane potential V, and a slow adaptation current w, which are governed by the following equations:

$$\begin{cases} \tilde{C}_m \frac{d\tilde{V}}{d\tilde{t}} = -\tilde{g}_L(\tilde{V} - \tilde{E}_L) + \tilde{g}_L \tilde{\Delta}_T \exp\left(\frac{\tilde{V} - \tilde{V}_{th}}{\tilde{\Delta}_T}\right) - \tilde{w} + \tilde{I}_e + \tilde{I}_s \\ \tilde{\tau}_w \frac{d\tilde{w}}{d\tilde{t}} = \tilde{a}(\tilde{V} - \tilde{E}_L) - \tilde{w} \end{cases} \tag{1}$$

$$\text{if } \tilde{V} > \tilde{V}_{peak} \quad \begin{cases} \tilde{V} & \leftarrow & \tilde{V}_r \\ \tilde{w} & \leftarrow & \tilde{w} + \tilde{b} \end{cases} \tag{2}$$

The main difference of this model compared to the integrate-and-fire model is the presence of the second variable $\tilde{w}$ which modulates the neuronal excitability. The synaptic input received by a neuron is represented by the variable $\tilde{I}_s$, which is usually time dependent. The neuronal adaptation can be either subthreshold, through the coupling between $\tilde{V}$ and $\tilde{w}$ via $\tilde{a}$, or spike-driven, from the step increments of size $\tilde{b}$ that $\tilde{w}$ undergoes after a spike.

In this study, and in accordance with the experimental observations for several types of pyramidal neurons, we will use only neuronal parameters leading to adapting neurons which exhibit periodic spiking. They are placed in a periodic spiking state through the persistent current $\tilde{I}_e$, which drives their progressive depolarisation and makes them spike periodically. Values of the parameters used for the AdEx model can be found in Table I, in the Appendices.

During the rest of the study, we will use the dimensionless version of the model:

$$\begin{cases} \dot{V} = -(V - E_L) + e^V - w + I_e + I_s \\ \tau_w \dot{w} = a(V - E_L) - w \end{cases} \tag{3}$$

Details for the change of variables are detailed in the Appendices, Neuronal model and parameters. From then on, all equations will involve only dimensionless parameters.

Synaptic model

The coupling strength between a pre-synaptic neuron A and a post-synaptic$B$, such that $A \to B$, is represented by the total charge Q_s transmitted from A to B. This charge is passed dynamically through the ion channels of the synapses, which we will represent here by an alpha-shaped post-synaptic current (PSC). This PSC is felt by B, after the arrival, at $t = 0$, of a spike emitted by A and described by:

$$I_s(t) = I_{AB}(t) = s_{AB} I_s(t) = s_{AB} I_0 t e^{-\frac{t}{\tau_s}}. \tag{4}$$

As such, the total charge delivered to B reads

$$Q_s = \int_0^\infty I_{AB}(t)dt = s_{AB} I_0 \tau_s^2. \tag{5}$$

In these two equations, s_{AB} is the strength of the synaptic connection from A to B, and $I_0 = \frac{1pA}{\tilde{g}_L \tilde{\Delta}_T}$ is the unit current which we set this way to be coherent with the conventions of the NEST simulator [11].

Network models

This study is based on two non-metric network models: a fully homogeneous network with fixed in-degree (FID) which will be useful to introduce the mean-field model, and more heterogeneous Gaussian in-degree (GID) networks which are supposed to be representative of connectivity in dissociated cultures [12].

The directed networks are generated using the following principles:

- in a FID graph, all neurons have the same number k of incoming connections, which are drawn at random from the the other existing neurons, thus leading to a binomial out-degree distribution;
- in the GID graph, for each neuron i, the incoming connections are similarly drawn in a random fashion, but the in-degree k_i is no longer identical for all neurons, but follows a Gaussian distribution with mean value $\overline{k}$ and standard deviation σ_k. The out-degree displays the same binomial distribution as the FID graph.

Note that the former can be seen as the limit case of the latter when the in-degree variance goes to zero.

All networks where generated using the graph-tool or igraph backends of the NNGT (Neural Networks' Growth and Topology) library.

Numerical simulations

All dynamical simulations were performed using the NEST simulator [11] using the `aeif_psc_alpha` model, which corresponds to the equations presented above. This model is present on the master branch of the GitHub repository or in release versions strictly higher than 2.11.0.

The neurons were set to adaptive spiking using the neuronal and synaptic parameters detailed in Table I and were connected using `static_synapse`s, i.e. without plasticity.

Simulations were started from a population of neurons in an asynchronous random state, with their state variable $\tilde{w}$ following a normal distribution of average value 50 pA and standard deviation 10 pA.

The runs were performed on local machines for 1000-neuron networks and on a BlueGene Q machine for larger networks, with size varying from 10k to 100k neurons. Unless specified, the average degree of the neurons was set to 100, which is the typical value estimated in neuronal cultures [12].

Activity analysis

Activity analysis was partly performed using tools from the NNGT library. The rest of the analysis tools are freely available on our GitHub repository.

In particular, the burst detection was set as follow:

- two spikes are considered as belonging to the same activity period if they are separated by less than 10 ms,
- the activity period is considered as a burst if at least 20% of the neurons in the network have been recruited.

Theoretical model

In order to study in details the properties of the activity and to provide an efficient way to predict the system's behavior without actually simulating the whole network, we derived a mean-field model that describes the system dynamics and predicts the range over which the characteristic frequencies can vary.

The model focuses on the fully synchronized dynamics, for which all neurons behave almost identically. The rationale of the model is most apparent if we first consider the case of a fixed in-degree network: as can be seen on Figure 1, once the population is synchronized, all neurons receive the same input: the effect of k simultaneous spikes, i.e. the sum of k PSCs. Since one neuron behaves exactly as any other neuron, this network of N neurons receiving k inputs of strength s is in fact equivalent to N isolated neurons, each one forming a close loop with one autapse – that is, a self-loop – of strength ks.

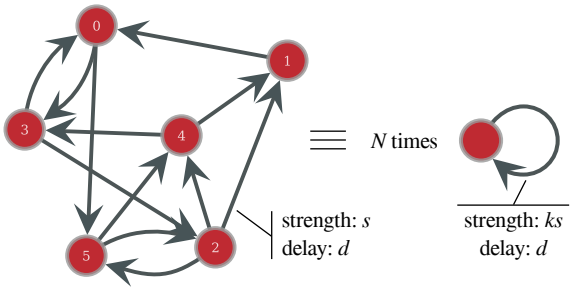


FIG. 1: Schematic representation of the equivalence between a FID network containing $N = 6$ synchronous neurons, with in-degree $k = 2$ and connection strength s, and N isolated neurons, with a self-loop connection of strength ks.

Based on this, we propose an Ansatz which reproduces the bursting dynamics for an "average" neuron and constrains this solution so that the resulting spiking activity of this neuron, excited by an equivalent, self-generated, input signal, drives the whole spike cascade of a burst and the successive recovery period. This restrains the evolution of the mean-field neuron, which must obey a specific self-consistent equation (SCE). Solving this equation, we obtain a complete description of the neuron's dynamical properties in time, which allows us to compute all the characteristics of the bursting dynamics.

In fact, the SCE implements a threshold condition which determines the burst termination and stops the fast increase of w; this is followed by a slow decrease of w which is reminiscent of the behavior of a relaxation oscillator. As the dynamics of w is slow except for its fast spike-triggered increase during the burst, our model is based on a quasi-static hypothesis regarding the subthreshold dynamics of w:

$$\tau_w \gg \tau_m = \frac{C_m}{g_L} = 1 \tag{6}$$

Details of the equations for the theoretical mean-field model are given in the Appendices.

Python tools to solve the self-consistent equation and compute the theoretical evolution of the neuronal state, as well as the characteristics of the bursts are freely available on our GitHub repository. The SCE is solved using the `scipy` implementation of Brent's root-finding method.

Exploration of parameter space

Thanks to the fast resolution of the equation in the mean-field model, we were able to compute the dynamical properties for a large number of parameter sets.

These results were normalized an analyzed through a PCA algorithm, using the `scikit.learn` package, in order to obtain the correlation matrix linking the collective dynamical properties to the precise values of the neuronal parameters.

For each parameter set, we first ensured that the model predicted a solution – i.e. the existence of bursts – then assessed the biological relevance of the solution using the following tests:

- rule out dynamics for which the voltage decreases to values lower than $-120\ mV$ during the giant hyper-polarization following a burst,
- restrict the maximum value of the slow current w to 1000 pA,
- prevent cellular bursting for individual neurons by asserting $V_r < V_{th}$ – this restricts the neurons to single-spike intrinsic behaviors [13].

These tests, constraining the number of "valid" parameter sets and making parameters interdependent, led to a non-trivial parameter/parameter correlation matrix, which is shown in the Appendices.

RESULTS

This study concerns a specific form of emergent synchronization leading to collective bursts. We will focus here on the fully synchronized state, without looking at the phase transition between the asynchronous and synchronous state, nor at the dynamic appearance of synchrony from an initially asynchronous system. However, we verified numerically that, for any given network, the synchrony indeed appears above a certain coupling strength.
This notion is very general in studies on synchronization, which are usually studied using the Kuramoto paradigm [14]. Though our model does not belong to this class, the coupling strength is also central here and is represented by the total charge Q_s delivered by a spike.

In all our simulations, regardless of the number of neurons involved, there exists a critical value $Q_{s,c}$ above which the neurons rapidly switch from their initially asynchronous state to a synchronous phase, thus converging to a dynamical attractor. This fast synchronization can be understood through an analogy with relaxation oscillators, which will be detailed in the next section, and is hinted at by the simple evolution of the slow variable w.

The attractor, inner structure of a burst

Once the network's dynamics becomes synchronous, it reaches an attractor composed of intermittent bursts of activity, which is shown in Figure 2 in the (V, w) phase space.

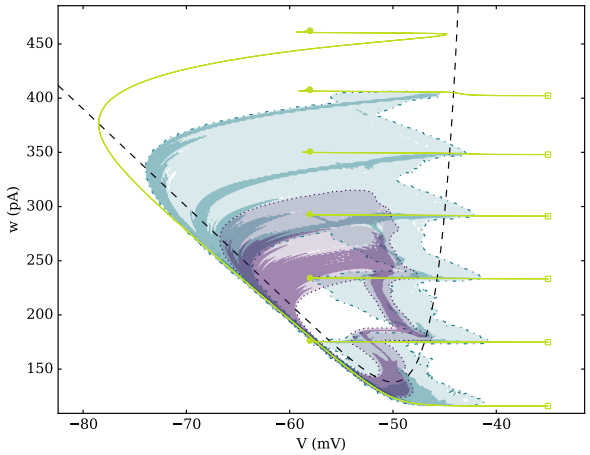


FIG. 2: Attractors for three different networks of 1000 identical neurons with average degree 100. Fixed-in-degree (FID) is represented by the green solid line (spike positions are represented by empty squares and reset positions by full circles). The resting V-nullcline – where $\dot{V} = 0$ for $I_s = 0$ – is given by the dashed curve. For Gaussian in-degree networks, the logarithm of the number of states per bin – over 200 simulations with 4 interbursts each – was used to compensate the non-constant velocity across the whole attractor. The larger attractor, in blue, is associated to $\sigma_k = 4$; the limit of one visit is marked by a dash-dot line. The smaller attractor, in purple, is for $\sigma_k = 20$ and is delimited by a dotted line. Bin size is approximately 0.05 mV along the V-axis and 1 pA along the w-axis.

This attractor is modified by the presence of heterogeneity in the network's topology – quantified by σ_k for GID networks – which impacts both its duration and regularity. Indeed, heterogeneity noticeably smooths the mean field behavior and reduces the number of spikes in a burst which goes down from 6 spikes per burst for the FID graph, to 3–5 if $\sigma_k = 4$, and is roughly reduced to 2 when $\sigma_k = 20$.

For the fully synchronized FID network, all neurons are responding to the exact same input – they receive spikes from the same number of neighbors – hence they are all equivalent to a mean-field neuron.
In this study, individual neurons are periodic spiking, a behavior that seems to originate from a persistent sodium current $I_{Na,p}$ in neuronal cultures [2], and is modeled here by a constant input current I_e.
When neurons are coupled, however, their periodic dynamics is drastically modified as they adopt a collective bursting behavior.

As can be seen on Figure 3, synchronized bursting of the population consists of a succession of active periods,

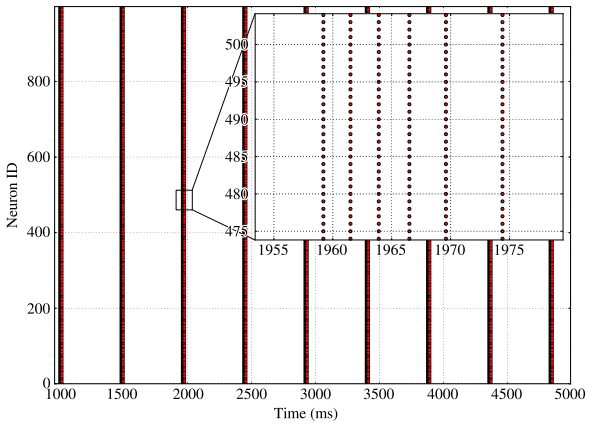


FIG. 3: Spike raster for a bursting 100-in-degree network. Inset provides detail for the behavior of the neurons during one burst, with successive SBSs separated by longer and longer intervals as the adaptation increases.

called *bursts*[1], separated by long inactive intervals, which we call recovery periods. As can be seen on the inset, the burst displays a strongly ordered inner structure composed of successive *synchronized burst slices* (SBS), which are consistent sets of spikes stemming from a common input.

Though this helps us define several quantities that characterize the dynamics such as the burst and inter-burst durations, information about the spike times alone is not sufficient to provide insight regarding the phenomena involved in the burst initiation or termination. Possible mechanisms for these two prominent steps will therefore be investigated based on the time evolution of the AdEx model state variables and phase-plane analysis.

Neuronal trajectory, assessment of the theoretical model

From the simulation, we can also record the evolution of V and w during the whole dynamics and thus reconstruct the trajectory of the neuronal state, either in time or in phase-space. Figure 4 **A** represents the time evolution of the average neuron during a bursting dynamics on a regular FID network and the comparison with the trajectory predicted by the theoretical mean-field model.
The close agreement between these trajectories shows that the theoretical model has a good predictive predictive. Indeed, the most visible discrepancy between the mean-field model and the simulations concerns the precise spike times, as shown in the inset of Figure 4 **A**; however, though the difference can be significant at the intraburst timescale, it is in fact limited to a few milliseconds, which is negligible compared to the period of the total phenomenon.

The dynamics can be understood most easily when looking at the behavior of w since the phenomenon can be seen as relaxation oscillations: the adaptation variable increases rapidly during the burst towards a peak value w^* – point (5) on the figure – then undergoes a quasi-exponential decrease until it reaches its minimum value w_{min} – point (4). Once this minimal value is reached, the neuron starts spiking, which makes w increase rapidly and the cycle starts again.

The evolution of V can then be seen as an interplay between the influence of w, I_e, and the synaptic currents in the active period:

- During the burst, each new spike induces a strong depolarisation of the membrane, thus leading to another spike – point (4) to (5) on the figure.
- Once w reaches its peak value w^*, its influence becomes predominant and prevents the neuron from firing; once the effect of the last spike vanishes, it drives a fast hyperpolarization of the neuron down to point (1).
- After V has reached a quasi-equilibrium value along its nullcline, it instantaneously adapts to the slow decay of w and increases progressively until the trajectory reaches the lowest point of the V-nullcline – point (3). This recovery from the strong hyperpolatization is greatly influenced by I_e.

[1] Let us insist once again that the term *burst* will always refer here to the concerted activity of a large fraction of the neuronal population and should not be confused with single neuron bursting behavior – though they share common characteristics – since they have different origins and population bursts occur on much longer timescales.

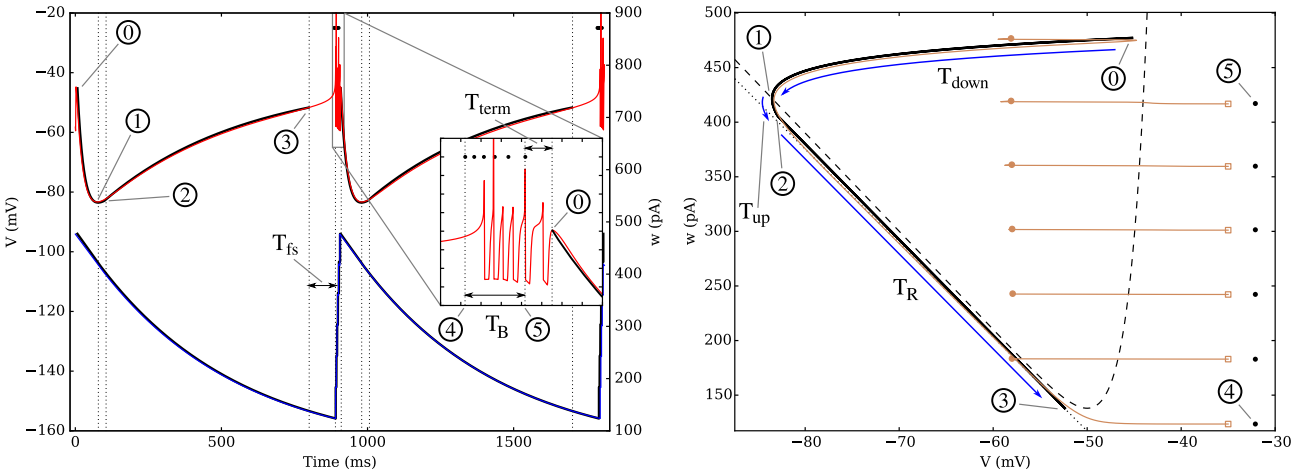


FIG. 4: **A**: time evolution of parameters V and w for the theoretical model (thick black lines) and for a simulation (thin red curve for V, blue for w) on a fixed in-degree graph with $k = 100$. Two bursts are represented and the intraburst dynamics is presented in the inset, where the spike times predicted by the mean-filed model are marked by black dots. The numbered circles mark the main points of the *theoretical* dynamics, where the behavior changes, as described in the Appendices. **B**: dynamics along the attractor in the phase plane for the same theoretical model (thick black curve) and simulation (thin brown). The three first periods following a burst are denoted by blue arrows: there is first a sharp decrease of V down to its minimum value as it crosses the nullcline (dashes); it is followed by a short interval where the neuronal state moves rapidly towards the "recovery curve" (dotted line), which is then followed until the minimum of the nullcline and the bursting sequence. The spike trajectory is cut on the figure (marked by empty squares) and the following reset point is marked by a filled circle. Neuronal and synaptic parameters are detailed in Table I, Set 1.

- At this point, the potential starts increasing more rapidly as the first spike is initiated until the bursting starts again with (4), where the first spike predicted by the mean-field model occurs.

Understanding the initiation and termination of a burst

One of the main interests of this mean-field model is that it provides an intuitive description of the phenomena responsible for both the initiation and the termination of the bursts. Indeed, as shown on Figures 4 **B** and 5, the whole existence of the short active period can be understood from the position of the neuronal state in phase space compared to the V-nullcline (the curve where $\dot{V} = 0$), which can be seen as an effective threshold.

The initiation of the burst simply occurs when w becomes low enough so that the trajectory can "pass under" the V-nullcline; this can be understood easily since the excitability of the neuron varies in the opposite direction as w. The lowest value w_{min} represent the situation where the excitability of the neuron has become so high that it spontaneously emits a spike.

To understand the succession of spikes during the burst and the reason why this spiking process eventually comes to an end without the need for inhibition or synaptic depression, we must first introduce a description of the dynamic coupling between the neurons.

The simplest way of modeling the effect of this coupling on the dynamics is to use Dirac synapses, since the arrival of a spike simply results in a step increment of the post-synaptic neuron's membrane potential:

$$V(t_{sp}^{+}) = V(t_{sp}^{-}) + \overline{k} Q_s \tag{7}$$

where t_{sp} is the time at which the spike is delivered to the post-synaptic neuron – t_{sp}^{-}/t_{sp}^{+} being respectively the instant immediately before/after – and Q_s is the total charge delivered by the spike, which reflects the coupling strength in the network.

The behavior of the neuron can easily be understood by looking at the situation in phase space on Figure 5. As the V-nullcline remains fix at all times[2]. Therefore, the condition for the occurrence of a new spike during the burst depends only on the position of $(V(t_{sp}^{+}), w)$ compared with the V-nullcline at this same value of w, $(V_{NV}(w), w)$, which is considered constant because of the quasi-static approximation on w. Hence, either $V(t_{sp}^{+}) > V_{NV}(w)$ and a new spike occurs, or $V(t_{sp}^{+}) \leq V_{NV}(w)$ and the burst terminates.

[2] The Dirac coupling being instantaneous, there is no finite time period where the effect of a post-synaptic current would modify the position of the V-nullcline

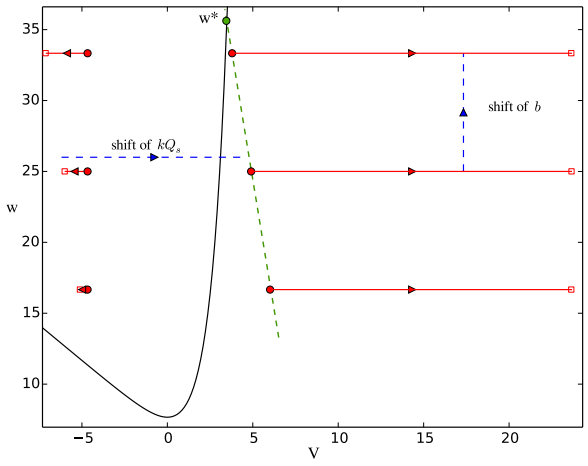


FIG. 5: Trajectory of a "Dirac burst" in dimensionless phase space. After a reset, the potential first decreases (leftmost parts of the trajectory) until the spike arrives (red square), at which point the potential is suddenly shifted to the corresponding red dot on the rightmost part of the trajectory. The decay before the spike arrival becomes more and more significant as w increases since it contributes negatively to $\dot{V}$. Burst continues until w becomes greater than w^*, denoted by the green dot, where the V-nullcline is crossed.

Summary of the theoretical description

Once we have computed w^* using the theoretical model, we can derive all the dynamical properties, starting with

$$w_{max} = \begin{cases} \left\lceil \frac{w^* - w_{min}}{b} \right\rceil b & \text{for FID networks} \\ w^* & \text{with heterogeneity} \end{cases} \tag{8}$$

This comes from the fact that, except when the neurons are exactly equivalent and synchronous – in which case they follow precisely the FID attractor, with w changing by discrete steps – the attractor has a less well defined boundaries, as shown on Figure 2; in this case, the mean $\langle w \rangle$ over the whole network has a smooth dynamics and w^* is closer to the statistical value at which the neurons stop bursting.

The complete dynamics of the model can be seen as relaxation oscillations with two phases: one resting period where the adaptation variable decreases until it reaches its lowest value and an active period where w increases rapidly up to its peak value. To be coherent with the results of [2], and reflect the periodicity of the system, we will define the inter-burst interval as

$$IBI = T_B + T_I. \tag{9}$$

This corresponds to the concatenation of the active period T_B and the resting period T_I, and shows a higher regularity in describing the phenomenon.
The resting period T_I can be approximated as the sum of the following terms:

T_{down} characterizes the time necessary for the neuron to undergo its strong hyperpolarization and reach its lowest membrane potential – point (1) on Figure 4,

T_R is the duration of the recovery – from (2) to (3),

T_{fs} is the time necessary for the initiation of the first spike which is roughly equivalent to the membrane time constant τ_m.

This allows us to obtain the characteristic values of the dynamics (see the Appendices for detailed calculations):

$$n_s = \left\lceil \frac{w^* - w_{min}}{b} \right\rceil \text{ (average number of spikes in a burst)},$$

$$T_B = \sum_{j=1}^{n_s - 1} t_s(w_{min} + jb), \text{ where } t_s(w) \text{ is the interspike interval (ISI) for a given value of } w,$$

$$T_{down} = \ln\left(\frac{\lambda}{\lambda - V_r + E_L + I_e - w_+} \right),$$

$$T_R = \frac{\tau_w}{\alpha\frac{a}{g_L}-1}\ln\left(\frac{\left(1-\alpha\frac{a}{g_L}\right)w_{min}-\frac{a}{g_L}(\beta-E_L)}{w_l(T_{down})\left(1-\alpha\frac{a}{g_L}\right)-\frac{a}{g_L}(\beta-E_L)}\right),$$

$$IBI = T_B + T_{down} + T_R + 1.$$

Because these results are analytic, thus immediate to compute, this has the significant advantage over simulations that it allows us to quickly predict the properties of the collective dynamics for a large number of parameter sets, i.e. of individual neuron's behaviors.

Evolution of the properties with neuronal and synaptic parameters

In order to assess the separate influence of the different neuronal parameters on the bursting properties, we used the model to test in a systematic way the influence of the separate variables.

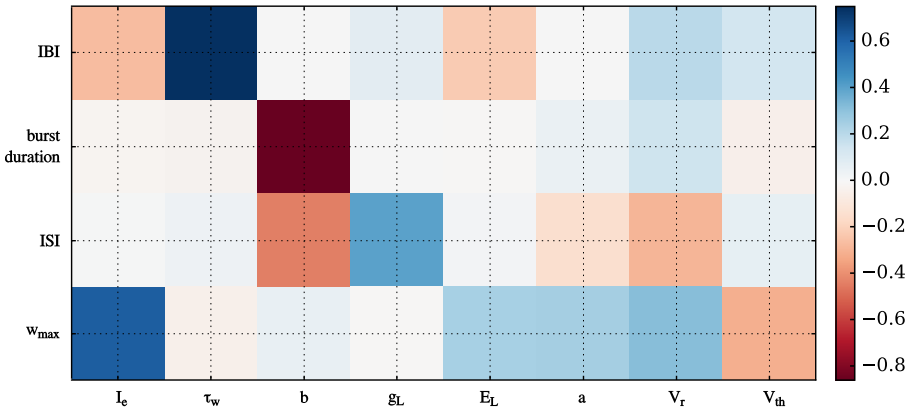


FIG. 6: Correlation matrix for the main characteristics of the bursting dynamics versus neuronal parameters. Correlations were performs over 50k randomly-drawn neuronal parameters sets using the predictions of the mean-field model.

As can be seen on Figure 6, this allows to compare the relative influence of any desired set of parameters in a fast and systematic way. Thus, it is a valuable tool to make preliminary explorations in order to prepare for subsequent experimental tests.

This matrix allows us to confirm obvious trends, such as the negative influence of the driving current I_e on the IBI, as it tends to quicken the depolarisation of the neurons. Likewise, τ_w is almost linearly related to the IBI since it dictates the decay time for w.

However, this systematic study also revealed less predictable correlations. Indeed, one of the most interesting features is the quasi-absence of influence of the subthreshold adaptation variable a compared to the spike-driven adaptation (characterized by b and V_r) on the most visible features of the activity, namely the IBI and burst duration.

DISCUSSION

Predictive ability of the model for heterogeneous networks

The first description of the model was given for a fully homogeneous FID network. However, as was already visible from Figure 2, the presence of heterogeneity in the network's structure has a significant influence on the period and firing rate of the bursting activity.

We provided the model with a simple way of taking this heterogeneity into account by tweaking the synaptic description.

Indeed, as the heterogeneity – namely σ_k – increases, the sharpness of the SBSs decreases until the spikes contained in the burst become more uniformly distributed; this is clearly visible on Figure 7, which show the comparison of a burst for two GID networks with different standard deviation on their in-degree distribution.

For very heterogeneous networks, the broad in-degree distribution leads the neurons to fire at seemingly random times during the bursting period. In the limit where the time distribution of the spikes inside a burst becomes completely uniform, we obtain a window-like synaptic current which is be zero during the interburst, then jump to a finite constant value during the burst.

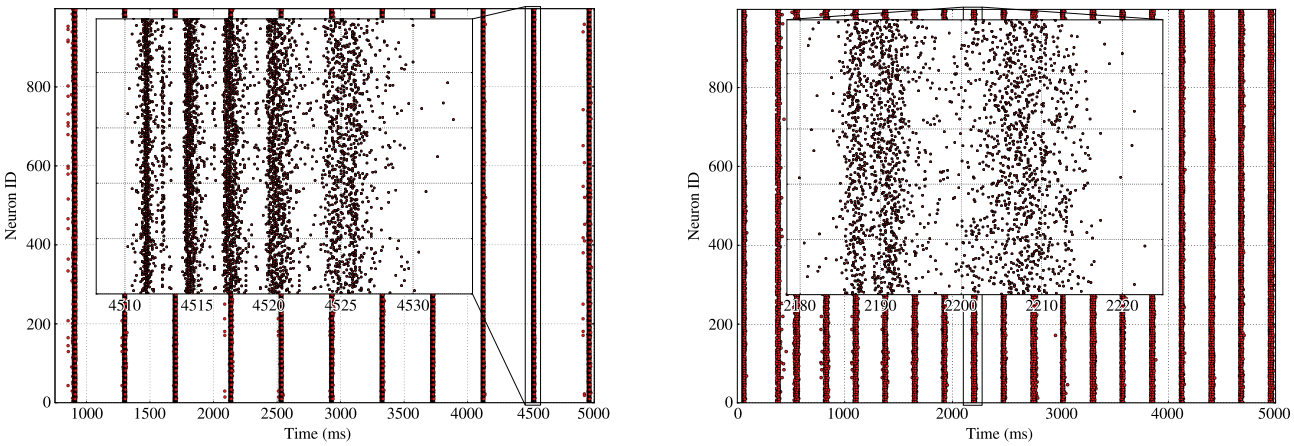


FIG. 7: Rasters of the bursting activity for 2 different Gaussian networks with 1000 neurons and an average in-degree of 100; each inset details the inner structure of a burst with the successive slices. **A)** Homogeneous GID network with $\overline{k} = 100$ and $\sigma_k = 5$ leads to well-defined SBSs inside the bursts. **B)** Heterogeneous GID network with $\overline{k} = 100$ and $\sigma_k = 20$ leads to fuzzy SBSs inside the bursts.

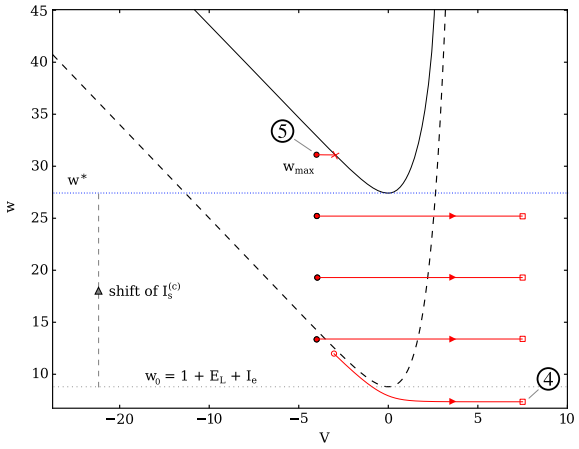


FIG. 8: Trajectory of a "continuous burst" in dimensionless phase space. Once the first spike occurs (marked by 4), the burst is initiated, i.e. a continuous current $I_s^{(c)}$ is injected into the neurons, thus shifting the resting V-nullcline (dashed curve) upwards (solid black). The neuron spikes until the last shift of b brings it above w^*, at w_{max}, where it encounters the nullcline, marking the end of the burst (5).

To obtain an effect equivalent to the spikes described in the Results subsection devoted the Dirac model, the total charge transmitted during the burst should be the same if an equal number of spikes is emitted. This condition reads, for an average in-degree $\overline{k}$ and a mean synaptic current $I_s^{(c)}$ during the burst,

$$I_s^{(c)} T_B = n_s \overline{k} Q_s. \tag{10}$$

As described previously, the burst termination occurs when the trajectory crosses the V-nullcline. Figure 8, this occurs as soon a w goes above the lowest point of the nullcline, for $w^* = 1 + E_L + I_s^{(c)} + I_e$. After a few lines of calculation detailed in the "Appendices: Bursting in heterogeneous networks" subsection (Eq. **??** to **??**), we obtain the self coherent equation:

$$w^* = w_{min} + b\left[\overline{t_s}(w^*) - d\right] + \overline{k} Q_s. \tag{11}$$

where $\overline{t_s}(w^*)$ is the average ISI in the burst.

Any real network should obviously fall in between the synchronous model with alpha-shaped synapses and this "continuous-synapses" model. This allows us to predict the interval in which the bursting properties should be contained, as shown on Figure 9.

Spike-triggered adaptation and its biological origin

Figure 6 showed a significant influence of the spike-triggered adaptation on the dynamics compared to the subthreshold adaptation, and a previous study [15] also hinted at the importance of a non-zero b value to obtain

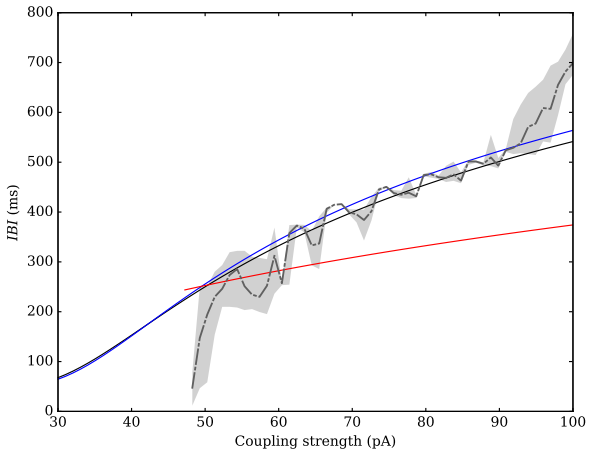


FIG. 9: Variation of the IBI depending on maximum value of the PSC (in pA). Mean-field predicted values are shown in solid blue, black and red respectively for the Dirac, alpha and continuous synaptic models. Simulated values for a Gaussian network with $\sigma_k = 4$ are represented in gray: the dash-dotted curve represents the average value and the grey fill marks the limit between the 5th and 95th percentiles.

low-frequency oscillations.
Using the mean-field model, this can be explained easily by the quasi-static hypothesis and the shape of Eq. (11). Indeed, the second term of the right-hand side involves the average ISI – which is an increasing function of w^* – and the spike-driven increment for the adaptation, b. Thus, the higher the effect of the spike-driven adaptation, the higher w^*, which leads to longer interbursts.
On the other hand, the quasi-static hypothesis states that the evolution of w is slow compared to that of V, meaning that the subthreshold variations given by a are limited by their slow evolution on a timescale of τ_w.

The assumption of a core population of oscillating, adaptive excitatory neurons is at the source of the bursting phenomena studied in this paper. Spontaneous, self-generated rhythmic neuronal activity has been recorded in a variety of cortical and thalamic networks as reviewd in [16] and has also been characterized in neuronal cultures [2]. These behaviors are generally assumed to involve a fraction of neurons which intrinsically exhibit periodic activity – i.e. even in the absence of external input. Intrinsic oscillatory firing of individual neurons has been suggested to rely on leak currents, which affect neuronal excitability [16] and particularly persistent non-inactivating sodium current $I_{Na,p}$ [17].

Adaptation, on the other hand is the property for some neurons stimulated by a rectangular current to exhibit periodic firing with a spiking frequency that progressively slows down from its initial high frequency value. More generally this phenomenon reveal the properties for periodic neurons to change, and more precisely to adapt, their oscillatory period. The biophysical processes mediating adaptation are thus possibly distinct for the origin of the rhythmic behavior which they modulate. Different slow K^+ polarizing currents seem indeed responsible for this frequency adaptation as the Muscarinic K^+ (I_M) current or the Ca^{2+} activated K^+ current (I_{AHP}) .

Spike triggered adaptation (the parameter b) summarizes the effect of calcium dependent potassium channels under the assumption that calcium influx occurs mainly during an action potential. Note that the coupling of voltage and adaptation via the parameter a also contributes to spike-triggered adaptation because of the sharp rise of the voltage during the upswing of an action potential.

Precision and validity range of the model

As the evolution of w is discontinuous, its the peak value changing by steps of b every time the number of spikes in a burst varies, comparison between the mean-field predictions and the simulations over a wide range of parameters can show significant increases of the relative error over small regions of the parameter-space. Indeed, a small difference between the predicted an simulated values can lead to a unit difference in the number of spikes in a burst, which leads to a sudden jump in the relative error, as the spikes' count is typically of the order of 10.

More importantly, as was stated at the beginning of this study, we focused on neurons displaying adaptive spiking; therefore, the mean-field model does not take into account the existence of intrinsically bursting behavior for some values of the neuronal parameters. Hence, in order to get meaningful results, one must take care to ensure that the sets of parameters used do not lead to that type of behavior, which is typically obtained when $V_r > V_{th}$ – see [13].

An additional limit of the model is apparent when the characteristic timescale of the synaptic rise time becomes of the order of magnitude of the spike propagation delay, since the model does not take PSCs overlap

into account.

Eventually, the conceptual boundaries of the model are reached in the limit of either a very weakly or very strongly coupled neuronal network.
The strong coupling limit is not the most troubling matter; indeed, the discrepancy between the mean-field model and the simulations mostly occur because the PSC becomes so intense that a single input can generate several spikes, which can occur *in silico* but has little biological relevance for adaptive spiking neurons.
The weak coupling limit, however, is more revealing: it shows that our model, designed to described a fully synchronous dynamics of bursts – i.e. active regions containing at least two spikes – cannot faithfully capture the smooth transition from an asynchronous state, which first involves oscillating firing rates, then synchronous slices containing only one spike, before bursts containing multiple spikes appear.

CONCLUSION

This study demonstrated the fact that a sufficient condition for synchronous bursting is the presence of a population of oscillating adaptive excitatory neurons. Furthermore, we showed that this leads to an emergent, drastic change of the neuronal behavior as they switch from a regular spiking to a collective bursting behavior.

We used a simple phase-space representation that helped us propose a mechanism for the initiation and termination of the bursting period related to spike-driven adaptation, which we link to the underlying biological phenomena. In addition, the derivation of an analytic mean-field model describing the complete bursting dynamics allowed us to predict the evolution of the characteristics of the global behavior from the properties of the individual units – neurons and synapses. Exploring a biologically relevant range for the neuronal parameters, we were able to reproduce a large range of biological rhythms with burst frequencies spanning almost 3 orders of magnitude from a few hundred milliseconds to tens of seconds, in accordance with experimental observation.

In our description, each new spike in the burst is cause by the previous one, which means that the delay between the emission of a spike and its reception by the post-synaptic neuron has a significant influence on the dynamics. Indeed, we understand intuitively that the longer the delay, the lower the excitability of the neurons when the PSC arrives, since the membrane potential can decay to lower values. This fact, added to the effect of heterogeneity in general – which tends to reduce the IBI length – hints a the existence of a limit to the spatial extension which can sustain coherent bursting.
Understanding the effect of heterogeneity and propagation delay will therefore constitute the logical continuation of this work. This could indeed explain the experimental observations in large cultures: MEA areas [2] exhibit strongly synchronous responses, while in larger cultures [4] the activity tends to initiate in specific regions – which would be able to sustain coherent bursts – before it propagates to the rest of the network.

Acknowledgments

We would like to thank Elisha Moses, Yaron Penn, and Menahem Segal for their help and the invaluable discussions we had, as well as for sharing their data with us; Hans Ekkehard Plesser for its help and thorough reviews during the implementation and improvements of the numerical models in NEST; Sylvie Thérond for helping with the installation of NEST on the Turing supercomputer.

This work was granted access to HPC resources from the IDRIS (Orsay) under the allocation 2016057701 made by GENCI (Grand équipement national de calcul intensif).

[1] J. M. Ramirez, A. K. Tryba, and F. Peña, Current Opinion in Neurobiology **14**, 665 (2004), ISSN 09594388.
[2] Y. Penn, M. Segal, and E. Moses, Proceedings of the National Academy of Sciences p. 201515105 (2016), ISSN 0027-8424, URL http://www.pnas.org/lookup/doi/10.1073/pnas.1515105113.
[3] S. T. Sipilä, K. Huttu, J. Voipio, and K. Kaila, European Journal of Neuroscience **23**, 2330 (2006), ISSN 0953816X, URL http://doi.wiley.com/10.1111/j.1460-9568.2006.04757.x.
[4] J. G. Orlandi, J. Soriano, E. Alvarez-Lacalle, S. Teller, and J. Casademunt, Nature Physics **9**, 582 (2013), ISSN 1745-2473, URL http://dx.doi.org/10.1038/nphys2686http://www.nature.com/doifinder/10.1038/nphys2686.
[5] T. Masquelier and G. Deco, PLoS ONE **8**, 1 (2013), ISSN 19326203.
[6] B. W. Connors and M. J. Gutnick, Trends in neurosciences **13**, 99 (1990), ISSN 01662236.
[7] D. Golomb, K. Donner, L. Shacham, D. Shlosberg, Y. Amitai, D. Hansel, C. Yue, and Y. Yaari, Journal of neurophysiology **96**, 1912 (2006), ISSN 0022-3077.
[8] T. A. Gritsun, J. Le Feber, J. Stegenga, and W. L. C. Rutten, Biological Cybernetics **102**, 293 (2010), ISSN 03401200.
[9] T. Gritsun, J. Le Feber, J. Stegenga, and W. L. C. Rutten, Biological Cybernetics **105**, 197 (2011), ISSN 03401200.

[10] R. Brette and W. Gerstner, J. Neurophysiol. **94**, 3637 (2005), ISSN 0022-3077, URL http://www.ncbi.nlm.nih.gov/pubmed/16014787.
[11] M.-O. Gewaltig and M. Diesmann, Scholarpedia **2**, 1430 (2007).
[12] O. Cohen, A. Keselman, E. Moses, J. Soriano, and T. Tlusty, EPL (Europhysics Letters) **89**, 1 (2010), ISSN 0295-5075, URL http://www.iop.org/EJ/abstract/0295-5075/89/1/18008/?rss=2.0.
[13] R. Naud, N. Marcille, C. Clopath, and W. Gerstner, Biological Cybernetics **99**, 335 (2008), ISSN 03401200.
[14] J. Acebrón, L. Bonilla, C. Vicente, F. Ritort, and R. Spigler, Reviews of Modern Physics **77** (2005), URL http://journals.aps.org/rmp/abstract/10.1103/RevModPhys.77.137.
[15] M. Augustin, J. Ladenbauer, and K. Obermayer, Frontiers in Computational Neuroscience **7**, 1 (2013), ISSN 1662-5188, URL http://journal.frontiersin.org/article/10.3389/fncom.2013.00009/abstract.
[16] G. T. Neske, Frontiers in Neural Circuits **9** (2016), ISSN 1662-5110, URL http://journal.frontiersin.org/Article/10.3389/fncir.2015.00088/abstract.
[17] H. Koizumi and J. C. Smith, The Journal of neuroscience : the official journal of the Society for Neuroscience **28**, 1773 (2008), ISSN 0270-6474.

APPENDICES

Neuronal model (AdEx) and parameters

The dimensionless parameters are obtained from their dimensional counterparts via the following formulas:

$$V = \frac{\tilde{V} - \tilde{V}_{th}}{\tilde{\Delta}_T}, \quad E_L = \frac{\tilde{E}_L - \tilde{V}_{th}}{\tilde{\Delta}_T} \quad \text{(general relation for voltages)}$$

$$w = \frac{w}{\tilde{g}_L \tilde{\Delta}_T}, \quad I = \frac{\tilde{I}}{\tilde{g}_L \tilde{\Delta}_T} \quad \text{(general relation for currents)}$$

$$t = \frac{\tilde{t}}{\tilde{\tau}_m}, \quad \tau_w = \frac{\tilde{\tau}_w}{\tilde{\tau}_m} \quad \text{(general relation for times)}$$

$$g_L = 1 \quad a = \frac{\tilde{a}}{\tilde{g}_L} \quad \text{(general relation for conductances)}$$

Throughout the numerical simulations, we restricted ourselves to a biologically relevant range for each parameters. These range, as well as two specific sets of parameters are detailed in Table I.

Parameter	Range	Set 1	Set 2
C_m	200	200	200
g_L	[4; 15]	9	9
E_L	$[-75; -65]$	-70	-70
V_{th}	$[-60; -45]$	-50	-50
V_r	$[-70; -50]$	-58	-58
I_e	[300; 600]	300	300
Δ_T	2	2	2
a	[0; 15]	2	2
τ_w	[300; 12000]	300	2000
t_{ref}	0	0	0
τ_s	[0.2; 0.8]	0.2	0.7
d	[1; 30]	1	5

TABLE I: Neuronal and synaptic parameters used in the simulations. The units are as follow: capacitance in pF, conductance in nS, voltage in mV, current in pA and time in ms. d is the spike transmission delay and t_{ref} is the value of the refractory period that can be set in the NEST simulator.

Though the ranges of the parameters are all biologically relevant, some combinations are not; thus, during the phase space exploration we performed, we ruled out the sets that led to either non algebraic values in the self-consistent equation, or non-plausible values for one of the dynamical characteristics. This led to the following correlation matrix for the parameters.

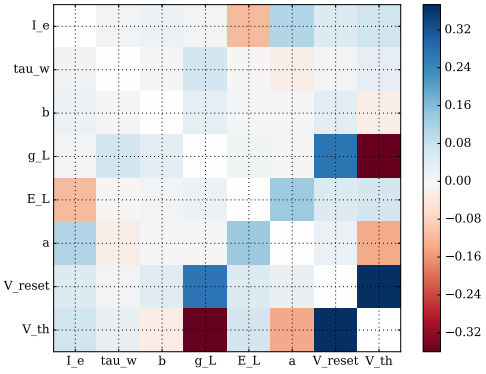


FIG. 10: Correlation matrix for the parameters (50k randomly-drawn neuronal parameters sets) after the tests for non-algebraic or non-biological values were performed.